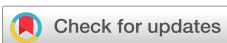


RESEARCH ARTICLE | MARCH 26 2025

Control of open quantum systems: The nonequilibrium Green's function perspective

Haoran Sun  ; Michael Galperin  

APL Quantum 2, 016134 (2025)

<https://doi.org/10.1063/5.0260691>View
OnlineExport
Citation

Articles You May Be Interested In

Quantum optimal control for pure-state preparation using one initial state

AVS Quantum Sci. (October 2021)

Robustness of dynamic quantum control: Differential sensitivity bounds

AVS Quantum Sci. (July 2024)

Unifying methods for optimal control in non-Markovian quantum systems via process tensors

J. Chem. Phys. (September 2024)

Control of open quantum systems: The nonequilibrium Green's function perspective

Cite as: APL Quantum 2, 016134 (2025); doi: 10.1063/5.0260691

Submitted: 26 January 2025 • Accepted: 6 March 2025 •

Published Online: 26 March 2025



View Online



Export Citation



CrossMark

Haoran Sun¹ and Michael Galperin^{2,a)}

AFFILIATIONS

¹ Department of Chemistry and Biochemistry, University of California San Diego, La Jolla, California 92093, USA

² School of Chemistry, Tel Aviv University, Tel Aviv 6997801, Israel

^{a)} Author to whom correspondence should be addressed: mgalperin@tauex.tau.ac.il

ABSTRACT

Manipulations with open quantum systems (such as qubits) are fundamental for any quantum technology. They are the focus of studies involving optimal control theory. Usually, control is achieved through the use of time-dependent external fields when driven system evolution is simulated employing the Davies construction (second-order Markov quantum master equation formulation). As a weak (second order) coupling scheme, the Davies construction is limited in its ability to account for bath-induced coherences. To overcome the limitation, we utilize the nonequilibrium Green's function method and demonstrate that accounting for the coherences makes a qualitative impact on quantum control studies. We find that accounting for the coherences is especially important when dealing with system evolution involving mixed states.

© 2025 Author(s). All article content, except where otherwise noted, is licensed under a Creative Commons Attribution (CC BY) license (<https://creativecommons.org/licenses/by/4.0/>). <https://doi.org/10.1063/5.0260691>

Optimal control deals with the task of achieving a desired quantum state of a system in an optimal way. Usually, control is achieved by employing time-dependent external fields. Historically, the field started with the consideration of isolated systems (e.g., molecules in gas phase), dynamics of which is described by the time-dependent Schrödinger equation. With the development of experimental capabilities, the attention of researchers has shifted to open quantum systems (e.g., qubits). Traditionally, almost all practical simulations employ the Davies construction to describe their dynamics. Limitations of the latter method include (among other restrictions) inability to account for bath-induced coherences. The latter is of central importance for any quantum control scheme. Here, we use NEGF as a method for describing the dynamics of a qubit. Its accuracy in accounting for coherences leads to qualitative differences in quantum control protocol when system evolution involves mixed states.

I. INTRODUCTION

Ability to create, transfer, and read quantum information is the foundation of quantum measurement,¹ quantum metrology,² and quantum computing.^{3,4} Corresponding ways and bounds

of information manipulations are discussed in the research on quantum steering,⁵ quantum resource theories,⁶ and quantum thermodynamics.^{7–9} In particular, fast and reliable reset of a qubit is the key prerequisite for any quantum technology.^{10,11} Implementation of the manipulations in physical systems is the focus of studies in quantum optimal control theory (OCT).^{12–17}

Optimal control deals with a task of achieving a desired quantum state of a system in an optimal way. Usually, control is achieved through the use of time-dependent external fields. Originally, optimal control theory was focused on isolated quantum systems, so that Schrödinger equation was the law describing the system's evolution.^{18–26} Effective computational algorithms to reach the desired outcome for such systems are available in the literature.^{27,28}

Realistic experimental setups deal with open quantum systems. Necessity to account for open character of the system led to modifications in OCT studies. First, a surrogate Hamiltonian approach was suggested.^{29–33} Within the approach, Schrödinger equation is applied to a finite surrogate Hamiltonian, which replaces physical (infinite) system–bath description. This finite representation is designed to generate reasonable short time dynamics of the system coupled to an infinite bath.

To simulate longer trajectories and incorporate correct thermodynamic behavior, open character of the system should be taken

into account more accurately. This resulted in substituting the Schrödinger equation with quantum master equation (QME) as the dynamical law in OCT studies. Because optimization relies on an iterative procedure, QME is usually taken in its most basic (Davies construction) form. Following tradition, OCT considerations with QME as the dynamical law ignore the influence of the time-dependent field on the dissipator.^{34–43} Later, to make modeling more realistic, the field's effect on the dissipator was taken into account within instantaneous (adiabatic) approximation.^{44,45}

Markov evolution simulated within the Davies construction is not always accurate in the prediction of open system responses.^{46,47} So, non-Markovian OCT was carried out for spin-boson system within the hierarchical equation of motion approach (HEOM).⁴⁸ HEOM is a very promising technique for the simulation of time-dependent and transient processes because of its linear scaling with time. Early versions of HEOM were limited to high temperatures and specific band structures. Later developments enable trading some of its advantage for greatly improved access to more general band structures and lower temperatures.⁴⁹ Still, it is not clear if experimentally relevant low temperatures are within reach of the technique.

Green's function methods⁵⁰ are capable of overcoming limitations of the techniques used in OCT literature so far. Here, we employ nonequilibrium Green's function (NEGF) method in OCT studies of a qubit. Following Ref. 45, we consider optimization of laser pulse with the goals of heating, cooling, and particular state preparation of an open quantum system. We compare QME results to more general NEGF simulations. We note that there are two aspects of quantum control analysis: 1. optimal control method and 2. theoretical approach used to describe evolution of the system. In our study, we follow the optimal control method employed in Ref. 45. While more advanced optimization methods are available in OCT literature, the focus of our consideration is the description of evolution of the system. We suggest the NEGF approach exemplified here and^{46,47} in non-Markovian scenarios of strong driving/coupling, where the usual Markovian (Davies construction) approaches become inaccurate. In those cases, NEGF could be a way around solving the non-Markovian integro-differential equations with memory kernels. In addition to preserving complete positivity of the system density operator,⁵¹ NEGF is capable of proper description of system–bath interaction including quantum effects (bath-induced coherences) and influence of time-dependent driving on the coupling. In this sense, choice of the optimization procedure is of secondary importance.

The structure of this paper is as follows: Section II introduces the model and describes methods used in simulations. Comparison between numerical results of QME and NEGF simulations is presented in Sec. III. Section IV summarizes our findings.

II. METHOD

Here, we introduce the model, discuss the optimization procedure, and describe methods employed in simulations of the system dynamics.

A. Model

Following Ref. 45, we consider a qubit S coupled to thermal bath B and driven by external time-dependent field $\epsilon(t)$ (see Fig. 1),

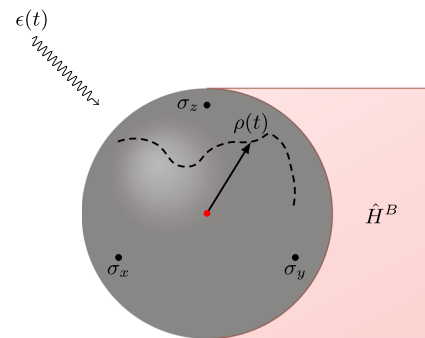


FIG. 1. Sketch of a qubit coupled to the thermal bath and driven by an external field.

$$\hat{H}(t) = \hat{H}_S(t) + \hat{H}_B + \hat{H}_{SB}, \quad (1)$$

where $\hat{H}_S(t)$ and \hat{H}_B describe the decoupled system and bath, respectively. \hat{H}_{SB} introduces interaction between them. Explicit expressions are (here and below $\hbar = k_B = 1$)

$$\hat{H}_S(t) = \sum_{i=1}^2 \Delta \hat{n}_i + \frac{\Delta}{2} (\hat{d}_1^\dagger \hat{d}_2 + \text{H.c.}) + \frac{\epsilon(t)}{2} (\hat{n}_2 - \hat{n}_1), \quad (2)$$

$$\hat{H}_B = \sum_{\alpha} \omega_{\alpha} \left(\hat{a}_{\alpha}^\dagger \hat{a}_{\alpha} + \frac{1}{2} \right), \quad (3)$$

$$\hat{H}_{SB} = \frac{i}{2} (\hat{d}_2^\dagger \hat{d}_1 - \hat{d}_1^\dagger \hat{d}_2) \sum_{\alpha} g_{\alpha} (\hat{a}_{\alpha} + \hat{a}_{\alpha}^\dagger). \quad (4)$$

Here, \hat{d}_i^\dagger (\hat{d}_i) and \hat{a}_{α}^\dagger (\hat{a}_{α}) create (annihilate) electrons in level i ($i = 1, 2$) and excitation in mode α of the thermal bath, respectively. $\hat{n}_i \equiv \hat{d}_i^\dagger \hat{d}_i$ is the particle number operator. The driving field $\epsilon(t)$ is modeled as a set of harmonic modes acting within a finite time interval,

$$\epsilon(t) = \exp \left[- \left(\frac{t - t_c/2}{t_c} \right)^2 \right] \sum_{k=1}^M c_k \sin(\nu_k t), \quad (5)$$

where M is the number of harmonic modes in the signal and t_c is the control time.

Note that the Hamiltonian commutes with the system total particle number operator,

$$[\hat{H}(t), \hat{n}_1 + \hat{n}_2] = 0. \quad (6)$$

Thus, the formulation properly describes qubit (spin-1/2) evolution when confined to the one-particle subspace.

B. Optimal control

There are two aspects to quantum control analysis: 1. optimal control method and 2. theoretical method describing evolution of the system.

In our analysis, we follow the optimal control method employed in Ref. 45. That is, the control objective is defined solely in terms of system observables, which are subject to environmental

influence. In the following, we consider several control tasks: reaching a particular quantum state (reset), heating, and cooling of the system. The tasks are achieved by optimization of the driving force profile $\varepsilon(t)$. In particular, we use coefficients c_k in the Fourier series (5) as adjustable parameters to minimize the cost functions, while frequencies ν_k are fixed,

$$\nu_k = \frac{k\pi}{t_c}, \quad k = 1, 2, 3, \dots \quad (7)$$

We start from decoupled qubit and bath, with the qubit being in an initial state $\hat{\rho}_i = \hat{\rho}(t=0)$. Within a predefined finite control time t_c , we search for such driving force profile $\varepsilon(t)$ that by the time $t = t_c$ the qubit evolves to some desired state $\hat{\rho}_f \approx \hat{\rho}(t_c)$. Note that density operator of a qubit can be decomposed as

$$\hat{\rho} = \left(\frac{1}{2} + x\hat{s}_x + y\hat{s}_y + z\hat{s}_z \right). \quad (8)$$

Here, $\hat{s}_{x,y,z}$ are the spin-1/2 operators and x, y, z are numbers between -1 and 1 . That is, the state of the qubit is fully defined by vector (x, y, z) (Bloch vector) and can be represented as a point within the 3D unit sphere (Bloch sphere), while distance between the two states can be defined as distance between a pair of 3D vectors.

Quality of the control is defined by a cost function $R[\hat{\rho}_i, \varepsilon(t)]$. That is, the goal of optimization is finding functions $c_k(t)$, which minimize the cost function. In particular, for reset (r) and heating (h) tasks, the cost function is defined as the distance between the state of the system at the end of the trajectory, $\hat{\rho}(t_c)$, and desired outcome $\hat{\rho}_f$,

$$R_{r,h}[\hat{\rho}_i, \varepsilon(t)] \equiv \|\hat{\rho}_f - \hat{\rho}(t_c)\|. \quad (9)$$

The cost function for cooling (c) task is defined as

$$R_c[\hat{\rho}_i, \varepsilon(t)] \equiv -\|\hat{\rho}(t_c)\|^2. \quad (10)$$

This form is used because of its faster convergence.

We note that the focus of our study is on the second aspect of control analysis. Clearly, proper description of system evolution is a prerequisite of any control scheme because the latter relies on dynamical trajectories generated during system evolution.

Qubit is a system weakly coupled to a thermal bath. Thus, there is a common belief in the optimal control community that the dynamics of such a system is adequately described within low-order (second in the system–bath coupling) quantum master equation (QME) formulation. In the following, we compare the advanced weak coupling QME scheme used in Ref. 45 to a more general nonequilibrium Green’s function formulation. We show that even in physically relevant weak coupling regime, low-order QME treatment may fail qualitatively. We now describe details of the QME and NEGF formulations and compare the two methods.

C. QME formulation

Following Ref. 45, for the standard OCT treatment, we simulate system evolution within the low-order QME formulation. We employ an advanced version of the QME where the effect of time-dependent driving field on the dissipation superoperator is taken

into account.⁵² Corresponding Markov EOM for system density operator in the interaction picture is (see Appendix A for details)

$$\begin{aligned} \frac{d}{dt}\hat{\rho}_S(t) = & \sum_m \left\{ -i \text{Im}(\Gamma_m(t)) [\hat{F}_m^\dagger(t)\hat{F}_m(t), \hat{\rho}_S(t)] \right. \\ & + 2\text{Re}(\Gamma_m(t)) [\hat{F}_m(t)\hat{\rho}_S(t)\hat{F}_m^\dagger(t) \right. \\ & \left. \left. - \frac{1}{2}\{\hat{F}_m^\dagger(t)\hat{F}_m(t), \hat{\rho}_S(t)\}\right] \right\}. \end{aligned} \quad (11)$$

Here, $\hat{F}_m(t)$ and $\Gamma_m(t)$ are the jump operators and time-dependent coefficients defined in Eqs. (A13) and (A5), respectively.

D. NEGF formulation

Single particle Green’s function,^{53,54}

$$G_{ij}(\tau_1, \tau_2) = -i\langle T_c \hat{d}_i(\tau_1) \hat{d}_j^\dagger(\tau_2) \rangle \quad (12)$$

is the central object to describe dynamics of the system within the NEGF. Here, $\tau_{1,2}$ are the Keldysh contour variables; T_c is the contour ordering operator; and $\hat{d}_i^\dagger(\tau)$ ($\hat{d}_i(\tau)$) is the electron creation (annihilation) operator in the Heisenberg picture. Single particle density matrix is given by the lesser projection of the Green’s function,

$$\rho_{ij}(t) \equiv \langle \hat{d}_j^\dagger(t) \hat{d}_i(t) \rangle = -i G_{ij}^<(t, t). \quad (13)$$

Within the NEGF, dynamics of the system is governed by the Kadanoff–Baym equation,

$$\begin{aligned} i \frac{\partial}{\partial \tau_1} G_{ij}(\tau_1, \tau_2) = & \delta_{ij} \delta(\tau_1, \tau_2) + \sum_m [H_S(t_1)]_{im} G_{mj}(\tau_1, \tau_2) \\ & + \sum_m \int_c d\tau \Sigma_{im}(\tau_1, \tau) G_{mj}(\tau, \tau_2). \end{aligned} \quad (14)$$

Here, t_1 is the physical time corresponding to contour variable τ_1 . Σ is the self-energy that describes the influence of the bath. Its explicit expression within the Hartree–Fock approximation is given in Eqs. (B4)–(B6).

E. Comparison between QME and NEGF formulations

It is important to note that second-order (in system–bath coupling) QME formulations are not accurate in several aspects:

1. Concept of weak coupling is not an absolute: if coupling can be considered as weak or strong depends on transport regime. Usually, one compares strength of system–bath interaction to distance between either levels of the unperturbed system or alignment between system and bath resonances. Thus, any coupling is strong at resonance. In this respect, low-order QME approaches can faithfully describe an off-resonant regime (secular approximation is used in this regime) or a strictly resonant situation (singular coupling limit is employed in this regime). However, the description of transition between the two regimes (for any system–bath coupling strength) is beyond their capabilities.
2. Second-order QME is not capable of properly describing bath-induced coherences; only populations are reproduced reliably.

Indeed, the lowest order contribution to the coherence is of fourth order, so it cannot be described by the second-order scheme.⁵⁵

Recently, it was realized in the optimal control community that the inability to describe bath-induced coherences by the low-order QME scheme may be important for developing the quantum control protocol. Reference 45 (which we follow and to which we compare) is an attempt to improve standard Davies construction⁵⁶ by introducing time dependence into the dissipation part of the Liouvillian, thus improving the scheme's ability to properly account for the system–bath coupling (that is, improving description of bath-induced coherences). However, the improvement still relies on the same weak (second order) coupling approximation and is done under Markovian assumption. This automatically makes the improvement limited in its ability to describe the coupling properly.

Nonequilibrium Green's function (NEGF) method treats system–bath coupling more accurately. Contrary to the low-order QME, it accounts for the coupling to infinite order (resummation of diagrams) and does not employ Markov approximation. Note that Markov QME can be derived from more general NEGF treatment by making Kadanoff–Baym-like approximation and neglecting retarded projection of the self-energy (this is the projection responsible for describing dissipation during system evolution).⁵⁷ Although NEGF can treat finite (strong) system–bath coupling, we intentionally focus on the parameter regime (weak coupling), which is physically relevant for qubit operation and which is favorable for the low-order QME scheme. Contrary to common belief in the quantum control community, even at weak coupling, accurate accounting for bath-induced coherences may lead to qualitative differences.

III. RESULTS

Time evolution within the QME formulation is numerically simulated using the Runge–Kutta method of fourth order (RK4).⁵⁸ Time propagation within the NEGF formulation is simulated following the scheme introduced in Ref. 59. The NEGF simulation employs fast Fourier transform (FFT), which is numerically performed utilizing the FFTW library.⁶⁰ Differential evolution⁶¹ is employed as the optimization algorithm to find driving force profile for both QME and NEGF dynamics; the same random generator, iterative depth, and population size are used in both cases.

In the following, we compare results of simulations within QME and NEGF for the optimized driving force $\varepsilon(t)$, entropy production $S_i(t)$, entropy $S(t)$, and cost function $R[\hat{\rho}_i, \varepsilon(t)]$. Entropy is obtained by integrating differential form of the second law of thermodynamics,

$$\frac{d}{dt}S(t) = \beta\dot{Q}_B(t) + \dot{S}_i(t), \quad \dot{S}_i(t) \geq 0, \quad (15)$$

where $\dot{Q}_B(t)$ and $\dot{S}_i(t)$ are heat flux between the qubit and thermal bath and entropy production rate, respectively. Heat flux is defined as rate of energy change in the bath,

$$\dot{Q}_B(t) = -\sum_{\alpha} \omega_{\alpha} \frac{d}{dt} \langle \hat{a}_{\alpha}^{\dagger}(t) \hat{a}_{\alpha}(t) \rangle. \quad (16)$$

Expressions for entropy and entropy production depend on the formulation of the second law. For systems weakly coupled to their baths (QME formulation), the former is given by the von Neumann expression,

$$S(t) = -\text{Tr}_S\{\hat{\rho}_S(t) \ln \hat{\rho}_S(t)\}, \quad (17)$$

which together with the expression for heat flux yields entropy production rate,⁶²

$$\begin{aligned} \dot{Q}_B(t) &= \text{Tr}_S\{(\mathcal{L}_D \rho_S(t)) \hat{H}^S(t)\}, \\ \dot{S}_i(t) &= -\text{Tr}_S\{(\mathcal{L}_D \rho_S(t)) \ln \hat{\rho}_S(t)\}. \end{aligned} \quad (18)$$

Here, \mathcal{L}_D is the dissipator part of the Liouvillian defined by the right side of Eq. (11).

For systems strongly coupled to their baths, we follow the formulation of Ref. 63. Expressions for heat flux and entropy production rate are

$$\begin{aligned} \dot{Q}_B(t) &= \int_0^{\infty} \frac{d\omega}{2\pi} \omega i_B(t, \omega), \\ \dot{S}_i(t) &= \int_0^{\infty} \frac{d\omega}{2\pi} \{ \phi^{out}(t, \omega) [\ln \phi^{out}(t, \omega) - \ln \phi^{in}(\omega)] \\ &\quad - (1 + \phi^{out}(t, \omega)) [\ln (1 + \phi^{out}(t, \omega)) - \ln (1 + \phi^{in}(\omega))] \}. \end{aligned} \quad (19)$$

Here, $i_B(t, \omega)$ is the energy resolved particle (phonon) flux between the system and thermal bath defined in Eq. (C9), and $\phi^{in}(\omega)$ and $\phi^{out}(t, \omega)$ are the thermal population of incoming and non-thermal population of outgoing states in the bath. Explicit expressions for the current and populations in terms of the Green's function (12) are given in Appendix C.

Parameters of the simulations are level separation Δ , Eq. (2), dissipation rate γ_0 and cutoff frequency of the bath spectral function [see Eqs. (B7)–(B9) for definitions], inverse temperature β , Eq. (B10), driving force number of modes M and bound on signal amplitude $\max|c_k|$, Eq. (5), size and step of the FFT grid, and maximum number of iterations employed by the optimization algorithm. Control time t_c is defined in each control task. In the following, all energies are presented in units of level separation Δ , and time unit is $1/\Delta$. The numerical values of the parameters are collected in Table I. We note that the parameters are favorable for applicability of the low-order QME formulation.

TABLE I. Parameters for numerical simulation.

Parameter	Value
Δ	1
γ_0	0.5
ω_c	5
β^{-1}	1
M	4
$\max c_k $	10
Size of the FFT grid	80 000
Energy step of the grid	π/t_c
Max number of iterations	10
Population size	15

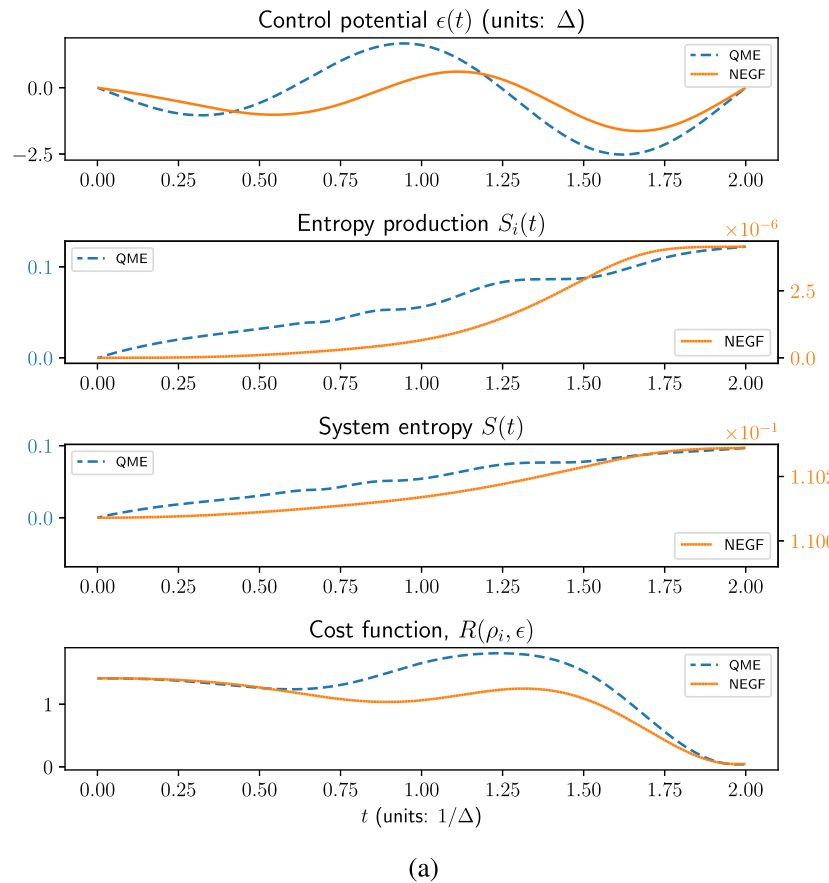
We now present the results of simulations within the QME and NEGF for reset, heating, and cooling of the qubit.

A. Reset

The system starts in an arbitrary pure state and the control goal is to bring it to a specific predefined pure state. As an example, we

consider system evolution from $\rho_i = (I + \sigma_z)/2$ to $\rho_f = (I - \sigma_x)/2$. Here, I is the identity matrix.

Figure 2 shows the results of simulations performed within QME and NEGF for $t_c = 2$. The performance of optimization within the two formulations is very similar. Qualitative behavior of the qubit response is the same [see panel (a)], with NEGF results demonstrating a slight time delay—a manifestation of the



(a)

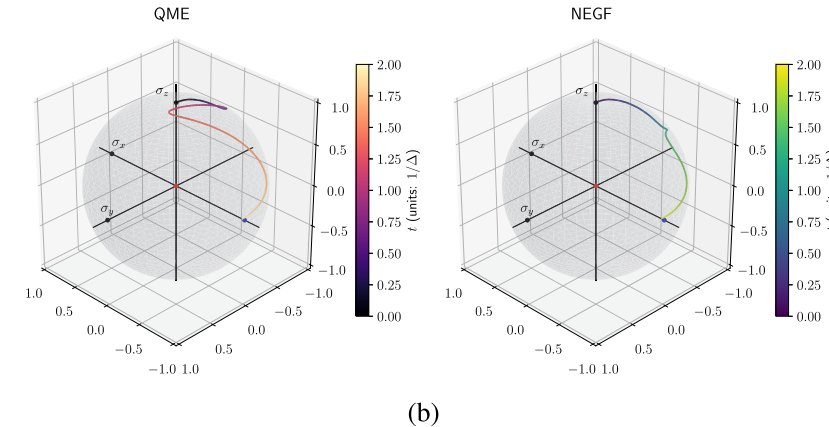
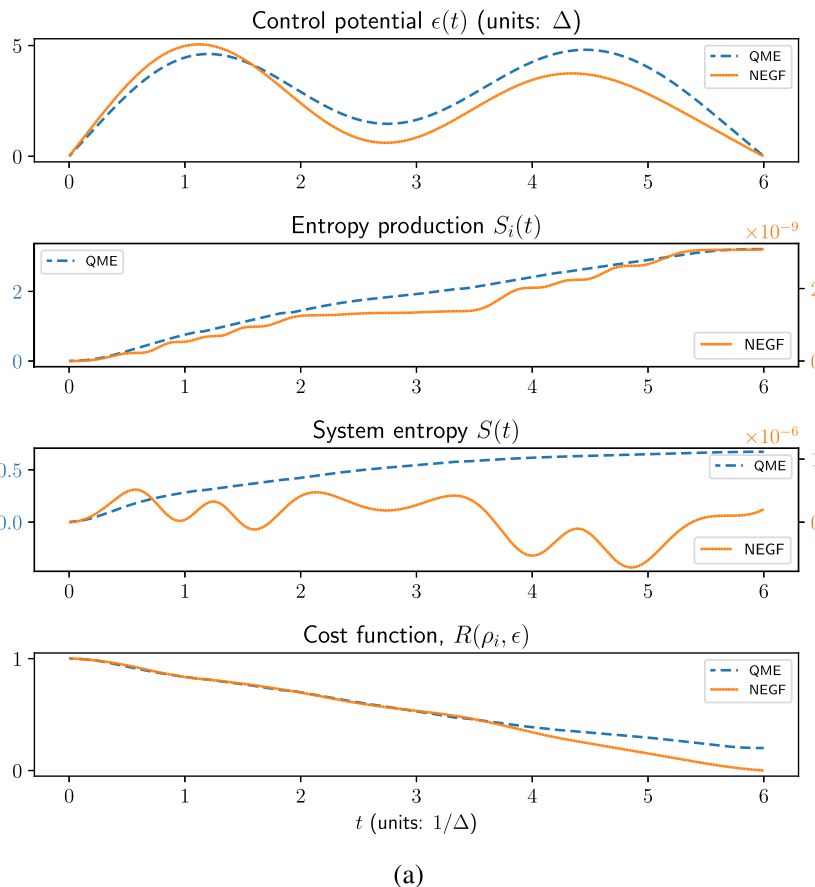


FIG. 2. Reset of the qubit: forced evolution from an arbitrary initial state ($\rho_i = (I + \sigma_z)/2$) to a predefined final state ($\rho_f = (I - \sigma_x)/2$). Panel (a) shows (top to bottom) optimal driving force potential, entropy production, entropy of the qubit, and cost function vs time simulated within QME (dashed line, blue) and NEGF (solid line, orange). Panel (b) shows trajectories of the system within the two formulations.

non-Markov character of the evolution. As expected, entropy production is seen to level by the end of the driving. Both schemes are capable of reaching the control goal with the same accuracy. Note that even trajectories [see panel (b)] are quite similar in short time for the two methods. This similarity is also observed in the other control tasks discussed in the following and is due to the

initial condition where qubit and the bath are decoupled. Such overall similarity of pure state to pure state transition is not surprising: with coupling to driving force much stronger than dissipation (which is a prerequisite for ability to control the qubit), dissipation almost does not play any role in a pure state evolution (note that both trajectories are confined to outer surface of the sphere),



(a)

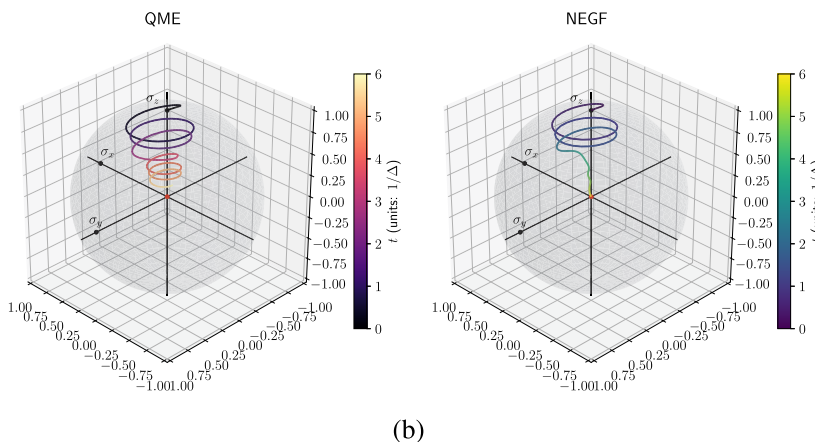


FIG. 3. Heating of the qubit: forced evolution from an arbitrary initial state ($\rho_i = (I + \sigma_z)/2$) to the maximum entropy state ($\rho_f = I/2$). Panel (a) shows (top to bottom) optimal driving force potential, entropy production, entropy of the qubit, and cost function vs time simulated within QME (dashed line, blue) and NEGF (solid line, orange). Panel (b) shows trajectories of the system within the two formulations.

while unitary evolution is the same under both QME and NEGF formulations.

B. Heating

Heating task is the process starting from a pure (cold) state evolving into the maximum entropy state, $\rho_f = I/2$. We choose the

initial (cold) state to be $\rho_i = (I + \sigma_z)/2$, which corresponds to $(0,0,1)$ vector on the sphere.

Figure 3 shows the results of simulations performed within QME and NEGF for $t_c = 6$. Contrary to the previous task, evolution involving mixed state demonstrates differences between the results of the two methods. Indeed, change from pure to mixed state is impossible without dissipation. The latter is treated very differently

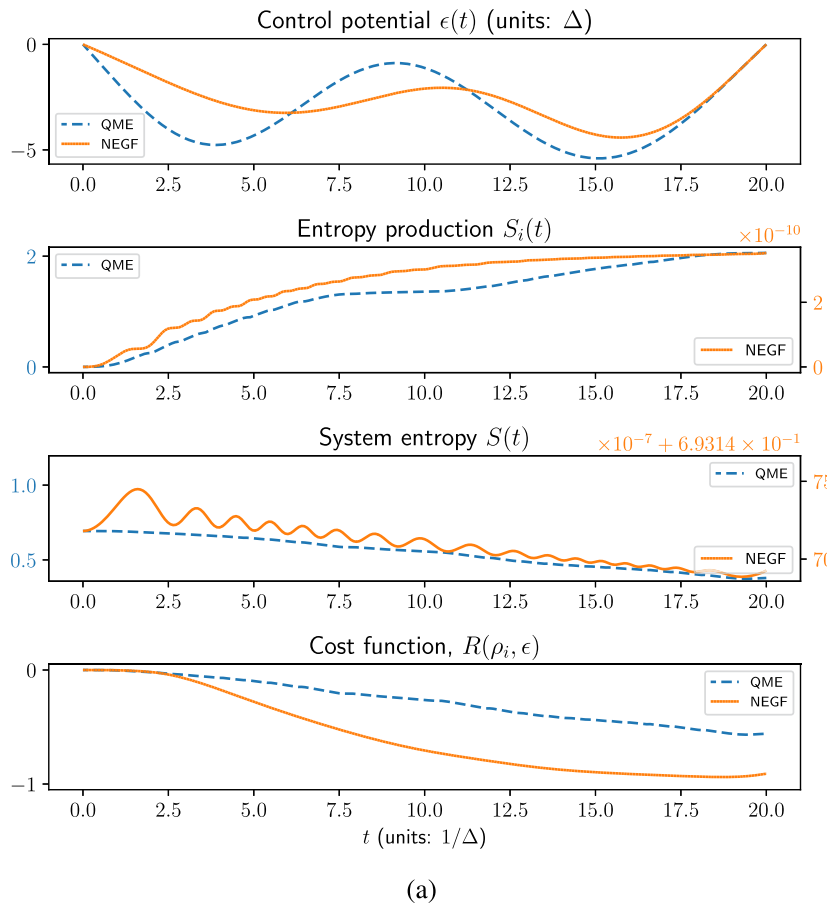
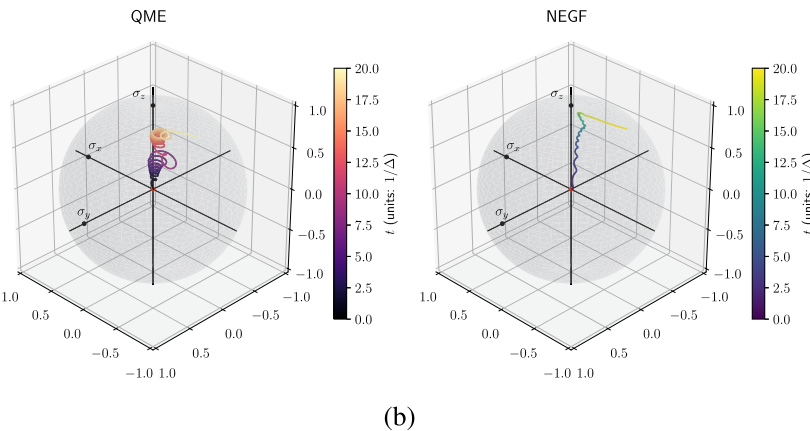


FIG. 4. Cooling of the qubit: forced evolution from the maximum entropy state ($\rho_i = I/2$) to a pure state ($\|\rho_f\| = 1$). Panel (a) shows (top to bottom) optimal driving force potential, entropy production, entropy of the qubit, and cost function vs time simulated within QME (dashed line, blue) and NEGF (solid line, orange). Panel (b) shows trajectories of the system within the two formulations.



within QME (Markov) and NEGF (non-Markov) formulations. This difference manifests itself in significant deviations of trajectories in the region where mixed character of the qubit is pronounced, that is deep inside the sphere [see panel (b)].

Note that NEGF simulation yields non-monotonic entropy change with possibility to have negative entropy values [see panel (a)]. Both effects are due to dynamics of entanglement formation between the system and bath during evolution and are a manifestation of non-negligible system–bath coupling (which is completely missed by the QME formulation).

In addition, note that for $t_c = 6$, NEGF is faster in reaching the final state [see the bottom graph in panel (a)]. Longer driving ($t_c = 12$, not shown) is necessary for the QME to achieve the same goal.

C. Cooling

Cooling is a process opposite to heating: the initial state is the maximum entropy state $\rho_i = I/2$, which evolves into a pure state ρ_f , where $|\rho_f| = 1$.

Figure 4 shows the results of simulations performed within QME and NEGF for $t_c = 100$. As with heating, the evolution involves mixed state, which leads to pronounced differences between QME and NEGF results. As previously, NEGF results demonstrate non-monotonic behavior of system entropy [see panel (a)] and drastically different trajectory [panel (b)]. Again, NEGF is much more efficient in reaching the final goal (the optimized cost function value is -0.64 for QME and -0.91 for NEGF). Note that simulations with longer driving ($t_c = 40$, not shown) also demonstrated superiority of the NEGF formulation. Moreover, increasing the number of iterations of the optimization cycle from 10 to 100 (not shown) did not affect inability of the QME to reach the final goal. Difficulty of the qubit to escape from a low purity state to a high purity state within QME (which is similar to the difficulty of the opposite process, as discussed above in heating task) is due to approximate (adiabatic) treatment of effect of the driving on system dissipation.

D. Discussion

Numerical results show that accurate accounting for coherences is crucial for the development of an optimal control protocol even in the weak system–bath coupling regime. This outcome is hardly surprising. Indeed, any quantum control method should carefully account for quantum coherences (note that coherences are the features that make quantum mechanics really quantum, otherwise—with only populations playing a role—one can describe the system within stochastic classical theory). In an open quantum system (e.g., qubit coupled to thermal bath), a part of those coherences comes from interaction of the system with its baths. Bath-induced coherences are not only space but also time-resolved quantities. While the main assumption of QME Markov schemes is infinitely fast bath dynamics, in reality, this is an idealization. Within the NEGF, bath-induced spatio-temporal correlations in the system are described by a two-time correlation function called self-energy

(its off-diagonal elements introduce time non-local bath induced coherences).

Numerical results show significant differences in the development of the quantum control protocol predicted by QME and NEGF methods. The most striking result (qualitative difference between Markov QME and non-Markov NEGF) is presented in **Fig. 4** (cooling task). Here, accounting for bath-induced coherences leads not only to numerical but also to qualitative difference in the predictions: while QME cannot reach the desired final state within the predefined time of evolution (driving signal), NEGF does provide such a possibility. We are cautiously inclined to say that the result is the best possible manifestation of importance of the bath-induced coherences, which are missed in the Markov low-order QME and accounted for by the NEGF.

IV. CONCLUSION

We consider manipulation of a qubit coupled to a thermal bath by an external driving field. Optimization of the field (time profile of the driving) has a goal of reaching a particular outcome (particular state of the qubit) for a fixed time of driving. We discuss three goals: reset (evolution from an arbitrary pure state to a predefined pure state of the qubit), heating (evolution from a pure state into the maximum entropy state, $\rho_f = I/2$, of the qubit), and cooling (evolution from the maximum entropy state, $\rho_f = I/2$, into a pure state of the qubit).

Usually, studies of optimization in open quantum systems employ the Davies construction to describe dynamics of the system. Among many limitations of the method, the most important for optimal control are either the absence of influence of time-dependent driving on the dissipator superoperator (in the standard formulation) or an approximate (adiabatic) way to account for the effect of the driving on dissipation (in generalized formulation).

We employ the NEGF where the effect of driving on dissipation is done more accurately and compare predictions of the two methods. We find that in evolution involving pure states (reset), the two formulations yield qualitatively similar results. This is due to the fact that any optimization task implies much stronger coupling to the driving field than to the bath. Thus, the effect of dissipation on dynamics, which is the part where the two methods are different, is minor. On the contrary, in evolutions involving mixed states (in particular, for transitions between pure and mixed states, as is the case in heating and cooling tasks), the two methods yield very different results, with the NEGF being more effective in reaching the desired goal. This is hardly surprising because any transition between pure and mixed state requires the presence of dissipation.

We note that our simulations were performed in a parameter regime favorable for employing the low-order QME formulations. Still, adiabatic approximation in treating the effect of time-dependent driving on dissipation within the method results in difficulties in describing mixed state evolution. This shows the superiority of non-Markovian Green's function techniques and hopefully will make those a tool of choice for studies of optimization in open quantum systems.

ACKNOWLEDGMENTS

We thank Ronnie Kosloff and Shimshon Kallush for helpful discussions. This material is based upon work supported by the National Science Foundation under Grant No. CHE-2154323.

AUTHOR DECLARATIONS

Conflict of Interest

The authors have no conflicts to disclose.

Author Contributions

Haoran Sun: Investigation (lead); Software (lead); Visualization (lead). **Michael Galperin:** Conceptualization (lead); Methodology (lead); Writing – review & editing (lead).

DATA AVAILABILITY

The data that support the findings of this study are available within the article.

APPENDIX A: DERIVATION OF EQ. (11)

Derivation of the time-dependent QME (11) follows the standard procedure for the Davies construction,⁶⁴ with the modification accounting for time-dependence of the driving field on the dissipator as is described in Ref. 45.

In particular, we start from the Redfield equation,

$$\frac{d}{dt} \hat{\rho}_S(t) = - \int_0^\infty ds \text{Tr}_B \left\{ \left[\hat{H}^{SB}(t), \left[\hat{H}^{SB}(t-s), \hat{\rho}_S(t) \otimes \hat{\rho}_B^{eq} \right] \right] \right\}. \quad (\text{A1})$$

Here, tilde indicates interaction picture, $\hat{\rho}_S(t)$ is the reduced density matrix of the qubit, and $\hat{\rho}_B^{eq}$ is the equilibrium density operator of the thermal bath. $\text{Tr}_B\{\dots\}$ is the trace over the bath degrees of freedom.

System–bath coupling (4) in the interaction picture is

$$\hat{H}^{SB}(t) \equiv \hat{U}_S^\dagger(t, 0) \frac{i}{2} \left(\hat{d}_2^\dagger \hat{d}_1 - \hat{d}_1^\dagger \hat{d}_2 \right) \hat{U}_S(t, 0) \otimes \hat{U}_B^\dagger(t, 0) \hat{B} \hat{U}_B(t, 0), \quad (\text{A2})$$

where $\hat{U}_S(t, 0)$ is the system free evolution operator, which satisfies

$$\frac{\partial}{\partial t} \hat{U}_S(t, 0) = -i \hat{H}^S(t) \hat{U}_S(t, 0), \quad (\text{A3})$$

$\hat{B} \equiv \sum_\alpha g_\alpha (\hat{a}_\alpha + \hat{a}_\alpha^\dagger)$, and $\hat{U}_B(t, 0)$ describes the evolution of free bath, which is assumed to be in thermal equilibrium.

Solving numerically free evolution (A3), one can introduce instantaneous eigenproblem for the operator $\hat{U}_S(t, 0)$,

$$\hat{U}_S(t, 0) |S(t)\rangle = e^{-i u_S(t)} |S(t)\rangle. \quad (\text{A4})$$

Here, $e^{-i u_S(t)}$ and $|S(t)\rangle$ are the eigenvalue and eigenvector, respectively. In the following, instantaneous eigenstates $\{|S(t)\rangle\}$ are used as a basis. Eigenvectors are used to define instantaneous jump operators,

$$\hat{F}_{S_1 S_2}(t) \equiv |S_1(t)\rangle \langle S_2(t)|, \quad (\text{A5})$$

which evolve as

$$\begin{aligned} \hat{U}_S^\dagger(t, 0) \hat{F}_{S_1 S_2}(t) \hat{U}_S(t, 0) &= e^{i[u_{S_1}(t) - u_{S_2}(t)]} \hat{F}_{S_1 S_2}(t) \\ &\equiv e^{-i\theta_{S_1 S_2}(t)} \hat{F}_{S_1 S_2}(t). \end{aligned} \quad (\text{A6})$$

These jump operators can be used to represent free evolution of any operator acting on system degrees of freedom only. In particular,

$$\hat{U}_S^\dagger(t, 0) \frac{i}{2} \left(\hat{d}_2^\dagger \hat{d}_1 - \hat{d}_1^\dagger \hat{d}_2 \right) \hat{U}_S(t, 0) = \sum_m \xi_m(t) e^{-i\theta_m(t)} \hat{F}_m(t), \quad (\text{A7})$$

where $m \equiv (S_1, S_2)$ indicates the transition between states of the system and $\xi_m(t)$ are the expansion coefficients of the result of evolution in the left side of (A7) in the basis of instantaneous jump operators (A5).

Using (A7) in (A1) leads to

$$\begin{aligned} \frac{d}{dt} \hat{\rho}_S(t) &= \sum_{m, m'} \int_0^\infty ds \xi_m^*(t) \xi_{m'}(t-s) e^{i[\theta_m(t) - \theta_{m'}(t-s)]} \\ &\times \left[\hat{F}_{m'}(t-s) \hat{\rho}_S(t) \hat{F}_m^\dagger(t) - \hat{F}_m^\dagger(t) \hat{F}_{m'}(t-s) \hat{\rho}_S(t) \right] \\ &\times \left\langle \hat{B}(t) \hat{B}(t-s) \right\rangle_{eq} + \text{H.c.}, \end{aligned} \quad (\text{A8})$$

where we used Hermitian property of \hat{s}_y , \hat{B} , Hamiltonian, and density operator, and where

$$\left\langle \hat{B}(t) \hat{B}(t-s) \right\rangle_{eq} \equiv \text{Tr}_B \left\{ \hat{B}(t) \hat{B}(t-s) \hat{\rho}_B^{eq} \right\}. \quad (\text{A9})$$

Standard derivation of the Davies construction implies an infinitely fast bath, this allows approximating

$$\xi_{m'}(t-s) \approx \xi_{m'}(t) \quad \text{and} \quad \hat{F}_{m'}(t-s) \approx \hat{F}_{m'}(t). \quad (\text{A10})$$

Expanding phase factor in (A8) to a linear term in time and employing rotating wave approximation (RWA),

$$\begin{aligned} \theta_m(t) - \theta_{m'}(t-s) &\approx \theta_m(t) - \theta_{m'}(t) + \omega_{m'}(t)s \\ &\approx \delta_{m, m'} \omega_m(t)s \end{aligned} \quad (\text{A11})$$

(here, second equality comes from the RWA assumption) leads to

$$\begin{aligned} \frac{d}{dt} \hat{\rho}_S(t) &= \sum_m \Gamma_m(t) \left[\hat{F}_m(t) \hat{\rho}_S(t) \hat{F}_m^\dagger(t) - \hat{F}_m^\dagger(t) \hat{F}_m(t) \hat{\rho}_S(t) \right] + \text{H.c.} \\ &= \sum_m \left\{ \text{Re}(\Gamma_m(t)) \left[\hat{F}_m(t) \hat{\rho}_S(t) \hat{F}_m^\dagger(t) + \hat{F}_m^\dagger(t) \hat{\rho}_S(t) \hat{F}_m(t) \right. \right. \\ &\quad \left. \left. - \left\langle \hat{F}_m^\dagger(t) \hat{F}_m(t), \hat{\rho}_S(t) \right\rangle \right] - i \text{Im}(\Gamma_m(t)) \left[\hat{F}_m^\dagger(t) \hat{\rho}_S(t) \right. \right. \\ &\quad \left. \left. \times \hat{F}_m(t) - \hat{F}_m(t) \hat{\rho}_S(t) \hat{F}_m^\dagger(t) + \left[\hat{F}_m^\dagger(t) \hat{F}_m(t), \hat{\rho}_S(t) \right] \right] \right\}, \end{aligned} \quad (\text{A12})$$

where

$$\Gamma_m(t) \equiv |\xi_m(t)|^2 \int_0^\infty ds e^{i\omega_m s} \left\langle \hat{B}(s) \hat{B}(0) \right\rangle_{eq}. \quad (\text{A13})$$

Taking into account that $\hat{F}_m(t)$ appears in (A12) as a result of expansion, Eq. (A7), of a Hermitian operator [that is, expansion in jump operators $\hat{F}_m(t)$ with coefficients $\xi_m(t)$ and phases $\theta_m(t)$] is equivalent to the expansion in jump operators $\hat{F}_m^\dagger(t)$ with coefficients $\xi_m^*(t)$ and phases $-\theta_m(t)$] expression (A12) reduces to Eq. (11).

APPENDIX B: QUBIT SELF-ENERGY DUE TO COUPLING TO THERMAL BATH

It is convenient to express system–bath coupling, Eq. (4), in a more general form

$$\hat{H}^{SB} = \sum_{ij} v_{ij} d_i^\dagger d_j \sum_\alpha g_\alpha (\hat{a}_\alpha + \hat{a}_\alpha^\dagger), \quad (B1)$$

where $v_{ij} = \frac{i}{2}(\delta_{i,2}\delta_{j,1} - \delta_{i,1}\delta_{j,2})$. The coupling is considered to be a perturbation. In the following, it is taken into account by employing diagrammatic expansion.

Rewriting the expression for single-particle Green’s function, Eq. (12), in the interaction picture,

$$G_{ij}(\tau_1, \tau_2) = -i \left\langle T_c \hat{d}_i(\tau_1) \hat{d}_j^\dagger(\tau_2) e^{-i \int_c d\tau \hat{H}^{SB}(\tau)} \right\rangle, \quad (B2)$$

expanding evolution operator up to second order in \hat{H}^{SB} , applying the Wick’s theorem, and dressing the diagrams yields the Dyson equation—integral form of the Kadanoff–Baym Eq. (14),

$$G_{ij}(\tau_1, \tau_2) = G_{ij}^{(0)}(\tau_1, \tau_2) + \sum_{l,m} \int_c d\tau \int_c d\tau' G_{il}^{(0)}(\tau_1, \tau) \times \Sigma_{lm}(\tau, \tau') G_{mj}(\tau', \tau_2), \quad (B3)$$

where $G^{(0)}$ is the single-particle Green’s function in the absence of the system–bath coupling and Σ is the self-energy due to the coupling. Explicit expression of the self-energy within the second-order expansion (the Hartree–Fock approximation) is

$$\Sigma_{lm}(\tau, \tau') = \underbrace{\Sigma_{lm}^H(\tau, \tau')}_{\text{Hartree}} + \underbrace{\Sigma_{lm}^F(\tau, \tau')}_{\text{Fock}}, \quad (B4)$$

$$\Sigma_{lm}^H(\tau, \tau') = -i\delta(\tau, \tau') \sum_{m'l'} \int_c d\tau'' v_{lm} v_{l'm'} G_{m'l'}(\tau'', \tau'_+) [\sigma(\tau'', \tau) + \sigma(\tau, \tau'')], \quad (B5)$$

$$\Sigma_{lm}^F(\tau, \tau') = i \sum_{m'l'} v_{lm} v_{l'm} G_{m'l'}(\tau, \tau') [\sigma(\tau', \tau) + \sigma(\tau, \tau')], \quad (B6)$$

where

$$\sigma(\tau, \tau') = -i \sum_\alpha g_\alpha^2 \left\langle T_c \hat{a}_\alpha(\tau) \hat{a}_\alpha^\dagger(\tau') \right\rangle_0. \quad (B7)$$

Here, $\langle \dots \rangle_0$ indicates free evolution of the bath.

In simulations, we will need lesser and greater projections of (B7). To obtain those, we start from energy domain, where

$$\begin{aligned} \sigma^<(\omega) &= -i\gamma(\omega)N(\omega), \\ \sigma^>(\omega) &= -i\gamma(\omega)[N(\omega) + 1] \end{aligned} \quad (B8)$$

and employ FFT. In (B8),

$$\gamma(\omega) = \gamma_0 \left(\frac{\omega}{\omega_c} \right)^2 e^{2(1 - \frac{\omega}{\omega_c})}, \quad (B9)$$

$$N(\omega) = \frac{1}{e^{\beta\omega} - 1} \quad (B10)$$

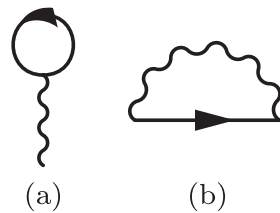


FIG. 5. Feynman diagrams of the self-energy (B4). (a) Hartree Σ^H , Eq. (B5), and (b) Fock Σ^F , Eq. (B6), contributions are shown.

are the dissipation rate and Bose–Einstein thermal distribution, respectively.

We note that because thermal bath (B8)–(B10) does not support zero frequency modes, only Fock self-energy, Eq. (B6), will contribute, as shown in Fig. 5.

APPENDIX C: NEGF EXPRESSIONS FOR THE HEAT FLUX AND ENTROPY PRODUCTION RATE

Here, we derive expressions for heat flux and entropy production rate of a qubit coupled to a thermal bath.

We start from considering the particle (phonon) flux on the system–bath interface. The flux is defined as the minus rate of change of population in the bath,

$$I_B(t) = -\frac{d}{dt} \sum_\alpha \langle \hat{a}_\alpha^\dagger(t) \hat{a}_\alpha(t) \rangle. \quad (C1)$$

For the Hamiltonian (1)–(4), it can be expressed in terms of mixed Green’s function,

$$I_B(t) = 2 \operatorname{Re} \left[\sum_\alpha g_\alpha G_{\alpha S}^<(t, t) \right], \quad (C2)$$

where Green’s function is the lesser projection of

$$G_{\alpha S}(\tau_1, \tau_2) \equiv -i \langle T_c \hat{a}_\alpha(\tau_1) \hat{S}^\dagger(\tau_2) \rangle. \quad (C3)$$

Here,

$$\hat{S} \equiv \frac{i}{2} (\hat{d}_2^\dagger \hat{d}_1 - \hat{d}_1^\dagger \hat{d}_2). \quad (C4)$$

Using the Dyson equation, mixed Green’s function is expressed in terms of free bath and system evolutions as

$$G_{\alpha S}(\tau_1, \tau_2) = \int_c d\tau F_\alpha^{(0)}(\tau_1, \tau) g_\alpha G_{SS}(\tau, \tau_2), \quad (C5)$$

where

$$F_\alpha^{(0)}(\tau_1, \tau_2) = -i \langle T_c \hat{a}_\alpha(\tau_1) \hat{a}_\alpha^\dagger(\tau_2) \rangle_0, \quad (C6)$$

$$G_{SS}(\tau_1, \tau_2) = -i \langle T_c \hat{S}(\tau_1) \hat{S}^\dagger(\tau_2) \rangle \quad (C7)$$

are Green’s functions describing the evolution of free bath phonon and full system excitation, respectively.

Substituting lesser projection of (C5) into (C2) leads to

$$I_B(t) = -2 \operatorname{Re} \int_0^t dt' \int \frac{d\omega}{2\pi} e^{-i\omega(t-t')} [\sigma^<(\omega) G_{SS}^>(t', t) - \sigma^>(\omega) G_{SS}^<(t', t)], \quad (\text{C8})$$

$$\equiv \int \frac{d\omega}{2\pi} i_B(t, \omega). \quad (\text{C9})$$

Here, $i_B(t, \omega)$ is the energy-resolved particle (phonon) flux and $\sigma^<$ is the Fourier transform of the lesser/greater projection of

$$\sigma(\tau_1, \tau_2) \equiv \sum_\alpha g_\alpha^2 F_\alpha^{(0)}(\tau_1, \tau_2). \quad (\text{C10})$$

Explicit expressions of the projections are given in Eq. (B8).

In terms of energy-resolved particle flux (C9), heat flux (which for the thermal bath is equivalent to energy flux) is

$$\dot{Q}_B(t) = \int_0^\infty \frac{d\omega}{2\pi} \omega i_B(t, \omega). \quad (\text{C11})$$

To derive the expression for entropy production, we express particle flux (C8) as the difference between incoming thermal and outgoing non-thermal fluxes. In writing this expression, we take into account that in 1D velocity exactly cancels with density of states.⁶⁵ Thus,

$$I_B(t) = \int \frac{d\omega}{2\pi} [\phi^{in}(\omega) - \phi^{out}(t, \omega)]. \quad (\text{C12})$$

Because expression for thermal population is known,

$$\phi^{in}(\omega) = N(\omega). \quad (\text{C13})$$

Equations (C12) and (C9) yield expression for outgoing non-thermal flux,

$$\phi^{out}(t, \omega) = \phi^{in}(\omega) - i_B(t, \omega). \quad (\text{C14})$$

The rate of entropy change is introduced as a difference between incoming and outgoing entropy fluxes,

$$\frac{dS}{dt} = \int \frac{d\omega}{2\pi} (\sigma[\phi^{in}(\omega)] - \sigma[\phi^{out}(t, \omega)]), \quad (\text{C15})$$

where

$$\sigma[\phi] \equiv -\phi \ln \phi + (1 + \phi) \ln (1 + \phi) \quad (\text{C16})$$

is the von Neumann expression for entropy in the bath. Finally, using (C11) and (C15) in (15) yields expression for entropy production,⁶³

$$\begin{aligned} \dot{S}_i(t) = & \int_0^\infty \frac{d\omega}{2\pi} \{\phi^{out}(t, \omega) [\ln \phi^{out}(t, \omega) - \ln \phi^{in}(\omega)] \\ & - (1 + \phi^{out}(t, \omega)) [\ln (1 + \phi^{out}(t, \omega)) - \ln (1 + \phi^{in}(\omega))]\}. \end{aligned} \quad (\text{C17})$$

Note that the consideration above is done in the diagonal approximation. General formulation can be found in Ref. 63.

REFERENCES

- ¹O. Gühne, E. Haapasalo, T. Kraft, J.-P. Pellonpää, and R. Uola, “Colloquium: Incompatible measurements in quantum information science,” *Rev. Mod. Phys.* **95**, 011003 (2023).
- ²G. Tóth and I. Apellaniz, “Quantum metrology from a quantum information science perspective,” *J. Phys. A: Math. Theor.* **47**, 424006 (2014).
- ³G. Adesso, T. R. Bromley, and M. Cianciaruso, “Measures and applications of quantum correlations,” *J. Phys. A: Math. Theor.* **49**, 473001 (2016).
- ⁴M.-L. Hu, X. Hu, J. Wang, Y. Peng, Y.-R. Zhang, and H. Fan, “Quantum coherence and geometric quantum discord,” *Phys. Rep.* **762–764**, 1–100 (2018).
- ⁵R. Uola, A. C. S. Costa, H. C. Nguyen, and O. Gühne, “Quantum steering,” *Rev. Mod. Phys.* **92**, 015001 (2020).
- ⁶E. Chitambar and G. Gour, “Quantum resource theories,” *Rev. Mod. Phys.* **91**, 025001 (2019).
- ⁷J. Goold, M. Huber, A. Riera, L. d. Rio, and P. Skrzypczyk, “The role of quantum information in thermodynamics—A topical review,” *J. Phys. A: Math. Theor.* **49**, 143001 (2016).
- ⁸S. Vinjanampathy and J. Anders, “Quantum thermodynamics,” *Contemp. Phys.* **57**, 545–579 (2016).
- ⁹R. Kosloff, “Quantum thermodynamics and open-systems modeling,” *J. Chem. Phys.* **150**, 204105 (2019).
- ¹⁰J. P. Palao and R. Kosloff, “Quantum computing by an optimal control algorithm for unitary transformations,” *Phys. Rev. Lett.* **89**, 188301 (2002).
- ¹¹S. Kallush and R. Kosloff, “Scaling the robustness of the solutions for quantum controllable problems,” *Phys. Rev. A* **83**, 063412 (2011).
- ¹²S. J. Glaser, U. Boscain, T. Calarco, C. P. Koch, W. Köckenberger, R. Kosloff, I. Kuprov, B. Luy, S. Schirmer, T. Schulte-Herbrüggen, D. Sugny, and F. K. Wilhelm, “Training Schrödinger’s cat: Quantum optimal control,” *Eur. Phys. J. D* **69**, 279 (2015).
- ¹³S. Deffner and S. Campbell, “Quantum speed limits: From Heisenberg’s uncertainty principle to optimal quantum control,” *J. Phys. A: Math. Theor.* **50**, 453001 (2017).
- ¹⁴M. Bukov, A. G. R. Day, D. Sels, P. Weinberg, A. Polkovnikov, and P. Mehta, “Reinforcement learning in different phases of quantum control,” *Phys. Rev. X* **8**, 031086 (2018).
- ¹⁵A. Frisk Kockum, A. Miranowicz, S. De Liberato, S. Savasta, and F. Nori, “Ultrastrong coupling between light and matter,” *Nat. Rev. Phys.* **1**, 19–40 (2019).
- ¹⁶D. Guéry-Odelin, A. Ruschhaupt, A. Kiely, E. Torrontegui, S. Martínez-Garaot, and J. G. Muga, “Shortcuts to adiabaticity: Concepts, methods, and applications,” *Rev. Mod. Phys.* **91**, 045001 (2019).
- ¹⁷C. P. Koch, U. Boscain, T. Calarco, G. Dirr, S. Filipp, S. J. Glaser, R. Kosloff, S. Montangero, T. Schulte-Herbrüggen, D. Sugny, and F. K. Wilhelm, “Quantum optimal control in quantum technologies. Strategic report on current status, visions and goals for research in Europe,” *EPJ Quantum Technol.* **9**, 1–60 (2022).
- ¹⁸A. P. Peirce, M. A. Dahleh, and H. Rabitz, “Optimal control of quantum-mechanical systems: Existence, numerical approximation, and applications,” *Phys. Rev. A* **37**, 4950–4964 (1988).
- ¹⁹R. Kosloff, S. A. Rice, P. Gaspard, S. Tersigni, and D. J. Tannor, “Wavepacket dancing: Achieving chemical selectivity by shaping light pulses,” *Chem. Phys.* **139**, 201–220 (1989).
- ²⁰T. Szakács, B. Amstrup, P. Gross, R. Kosloff, H. Rabitz, and A. Lörincz, “Locking a molecular bond: A case study of CsI,” *Phys. Rev. A* **50**, 2540–2547 (1994).
- ²¹J. P. Palao and R. Kosloff, “Optimal control theory for unitary transformations,” *Phys. Rev. A* **68**, 062308 (2003).
- ²²C. P. Koch, J. P. Palao, R. Kosloff, and F. Masnou-Seeuws, “Stabilization of ultracold molecules using optimal control theory,” *Phys. Rev. A* **70**, 013402 (2004).
- ²³J. P. Palao, R. Kosloff, and C. P. Koch, “Protecting coherence in optimal control theory: State-dependent constraint approach,” *Phys. Rev. A* **77**, 063412 (2008).
- ²⁴M. Tomza, M. H. Goerz, M. Musiał, R. Moszynski, and C. P. Koch, “Optimized production of ultracold ground-state molecules: Stabilization employing potentials with ion-pair character and strong spin-orbit coupling,” *Phys. Rev. A* **86**, 043424 (2012).
- ²⁵A. Aroch, S. Kallush, and R. Kosloff, “Optimizing the multicycle subrotational internal cooling of diatomic molecules,” *Phys. Rev. A* **97**, 053405 (2018).

- ²⁶I. Schaefer and R. Kosloff, "Optimization of high-order harmonic generation by optimal control theory: Ascending a functional landscape in extreme conditions," *Phys. Rev. A* **101**, 023407 (2020).
- ²⁷M. Ndong, H. Tal-Ezer, R. Kosloff, and C. P. Koch, "A Chebychev propagator for inhomogeneous Schrödinger equations," *J. Chem. Phys.* **130**, 124108 (2009).
- ²⁸M. Rossignolo, T. Reisser, A. Marshall, P. Rembold, A. Pagano, P. J. Vetter, R. S. Said, M. M. Müller, F. Motzoi, T. Calarco, F. Jelezko, and S. Montangero, "QuOCS: The quantum optimal control suite," *Comput. Phys. Commun.* **291**, 108782 (2023).
- ²⁹R. Baer and R. Kosloff, "Quantum dissipative dynamics of adsorbates near metal surfaces: A surrogate Hamiltonian theory applied to hydrogen on nickel," *J. Chem. Phys.* **106**, 8862–8875 (1997).
- ³⁰D. Gelman and R. Kosloff, "Minimizing broadband excitation under dissipative conditions," *J. Chem. Phys.* **123**, 234506 (2005).
- ³¹E. Asplund and T. Klüner, "Optimal control of open quantum systems applied to the photochemistry of surfaces," *Phys. Rev. Lett.* **106**, 140404 (2011).
- ³²E. Asplund and T. Klüner, "Optimal control of open quantum systems: A combined surrogate Hamiltonian optimal control theory approach applied to photochemistry on surfaces," *J. Chem. Phys.* **136**, 124118 (2012).
- ³³M. Abdelhafez, D. I. Schuster, and J. Koch, "Gradient-based optimal control of open quantum systems using quantum trajectories and automatic differentiation," *Phys. Rev. A* **99**, 052327 (2019).
- ³⁴A. Bartana, R. Kosloff, and D. J. Tannor, "Laser cooling of molecular internal degrees of freedom by a series of shaped pulses," *J. Chem. Phys.* **99**, 196–210 (1993).
- ³⁵H. Tang, R. Kosloff, and S. A. Rice, "A generalized approach to the control of the evolution of a molecular system," *J. Chem. Phys.* **104**, 5457–5471 (1996).
- ³⁶D. J. Tannor, R. Kosloff, and A. Bartana, "Laser cooling of internal degrees of freedom of molecules by dynamically trapped states," *Faraday Discuss.* **113**, 365–383 (1999).
- ³⁷Y. Ohtsuki, W. Zhu, and H. Rabitz, "Monotonically convergent algorithm for quantum optimal control with dissipation," *J. Chem. Phys.* **110**, 9825–9832 (1999).
- ³⁸A. Bartana, R. Kosloff, and D. J. Tannor, "Laser cooling of molecules by dynamically trapped states," *Chem. Phys.* **267**, 195–207 (2001).
- ³⁹R. Xu, Y. Yan, Y. Ohtsuki, Y. Fujimura, and H. Rabitz, "Optimal control of quantum non-Markovian dissipation: Reduced Liouville-space theory," *J. Chem. Phys.* **120**, 6600–6608 (2004).
- ⁴⁰G. Katz, M. A. Ratner, and R. Kosloff, "Decoherence control by tracking a Hamiltonian reference molecule," *Phys. Rev. Lett.* **98**, 203006 (2007).
- ⁴¹D. Basilewitsch, R. Schmidt, D. Sugny, S. Maniscalco, and C. P. Koch, "Beating the limits with initial correlations," *New J. Phys.* **19**, 113042 (2017).
- ⁴²D. Basilewitsch, C. P. Koch, and D. M. Reich, "Quantum optimal control for mixed state squeezing in cavity optomechanics," *Adv. Quantum Technol.* **2**, 1800110 (2019).
- ⁴³A. Aroch, R. Kosloff, and S. Kallush, "Employing typicality in optimal control theory: Addressing large Hilbert spaces," *Phys. Rev. A* **107**, 022603 (2023).
- ⁴⁴R. Dann and R. Kosloff, "Quantum thermo-dynamical construction for driven open quantum systems," *Quantum* **5**, 590 (2021).
- ⁴⁵S. Kallush, R. Dann, and R. Kosloff, "Controlling the uncontrollable: Quantum control of open-system dynamics," *Sci. Adv.* **8**, eadd0828 (2022).
- ⁴⁶M. Esposito, M. A. Ochoa, and M. Galperin, "Efficiency fluctuations in quantum thermoelectric devices," *Phys. Rev. B* **91**, 115417 (2015).
- ⁴⁷Y. Gao and M. Galperin, "Simulation of optical response functions in molecular junctions," *J. Chem. Phys.* **144**, 244106 (2016).
- ⁴⁸E. Mangaud, R. Puthumpally-Joseph, D. Sugny, C. Meier, O. Atabek, and M. Desouter-Lecomte, "Non-Markovianity in the optimal control of an open quantum system described by hierarchical equations of motion," *New J. Phys.* **20**, 043050 (2018).
- ⁴⁹A. Erpenbeck, C. Hertlein, C. Schinabeck, and M. Thoss, "Extending the hierarchical quantum master equation approach to low temperatures and realistic band structures," *J. Chem. Phys.* **149**, 064106 (2018).
- ⁵⁰G. Cohen and M. Galperin, "Green's function methods for single molecule junctions," *J. Chem. Phys.* **152**, 090901 (2020).
- ⁵¹M. J. Hyrkäs, D. Karlsson, and R. van Leeuwen, "Cutting rules and positivity in finite temperature many-body theory," *J. Phys. A: Math. Theor.* **55**, 335301 (2022).
- ⁵²R. Dann, A. Levy, and R. Kosloff, "Time-dependent Markovian quantum master equation," *Phys. Rev. A* **98**, 052129 (2018).
- ⁵³H. Haug and A.-P. Jauho, in *Quantum Kinetics in Transport and Optics of Semiconductors, Springer Series in Solid-State Sciences*, 2nd, substantially revised edition ed., edited by M. Cardona, P. Fulde, K. von Klitzing and H.-J. Queisser (Springer, Berlin, Heidelberg, 2008), Vol. 123.
- ⁵⁴G. Stefanucci and R. van Leeuwen, *Nonequilibrium Many-Body Theory of Quantum Systems: A Modern Introduction* (Cambridge University Press, 2013).
- ⁵⁵M. Leijnse and M. R. Wegewijs, "Kinetic equations for transport through single-molecule transistors," *Phys. Rev. B* **78**, 235424 (2008).
- ⁵⁶E. B. Davies, "Markovian master equations," *Commun. Math. Phys.* **39**, 91–110 (1974).
- ⁵⁷N. Seshadri, A. Li, and M. Galperin, "Liouvillian exceptional points of an open driven two-level system," *J. Chem. Phys.* **160**, 044116 (2024).
- ⁵⁸W. H. Press, S. A. Teukolsky, W. T. Vetterling, and B. P. Flannery, *Numerical Recipes in C: The Art of Scientific Computing* (Cambridge University Press, 1997).
- ⁵⁹A. Stan, N. E. Dahlen, and R. van Leeuwen, "Time propagation of the Kadanoff–Baym equations for inhomogeneous systems," *J. Chem. Phys.* **130**, 224101 (2009).
- ⁶⁰M. Frigo and S. G. Johnson, "The design and implementation of FFTW3," *Proc. IEEE* **93**, 216–231 (2005).
- ⁶¹R. Storn and K. Price, "Differential evolution—A simple and efficient heuristic for global optimization over continuous spaces," *J. Global Optim.* **11**, 341–359 (1997).
- ⁶²K. Ptaszyński and M. Esposito, "Thermodynamics of quantum information flows," *Phys. Rev. Lett.* **122**, 150603 (2019).
- ⁶³J. Zhou, A. Li, and M. Galperin, "Quantum thermodynamics: Inside–outside perspective," *Phys. Rev. B* **109**, 085408 (2024).
- ⁶⁴H.-P. Breuer and F. Petruccione, *The Theory of Open Quantum Systems* (Oxford University Press, Oxford, New York, 2003).
- ⁶⁵M. Büttiker, "Scattering theory of current and intensity noise correlations in conductors and wave guides," *Phys. Rev. B* **46**, 12485–12507 (1992).